Inorganic Chemistry

Article

pubs.acs.org/IC

A Novel Synthetic Route for the Preparation of an Amorphous Co/Fe Prussian Blue Coordination Compound with High Electrocatalytic Water Oxidation Activity

Merve Aksoy,[†] Satya Vijaya Kumar Nune,[†] and Ferdi Karadas*[,†,‡]

[†]Department of Chemistry and [‡]UNAM Institute of Materials Science and Nanotechnology, Bilkent University, 06800 Ankara, Turkey

Supporting Information

ABSTRACT: Co/Fe Prussian Blue coordination networks have recently been investigated for heterogeneous water oxidation catalysis. Despite their robustness and stability in both acidic and neutral media, the relatively low current density obtained is their main drawback as a result of their low surface concentration. A novel synthetic approach was employed using a pentacyanometalate-based metallopolymer for the preparation of amorphous Co/Fe coordination polymers to overcome this problem. The surface concentration was improved approximately 7-fold, which also resulted in an increase in the catalytic activity. A current density of 1 mA·cm^{-2} was obtained only at η = 510 mV, while the same current density could be obtained at higher overpotentials (>600 mV) with conventional Prussian Blue analogues. IR, X-ray photoelectron spectroscopy, and energy-dispersive X-ray spectroscopy studies were performed to investigate the stability of electrodes before and after the electrocatalytic process. The results of this study indicate that the rich and diverse chemistry of pentacyanometalates makes them potential candidates for application in heterogeneous water oxidation catalysis.

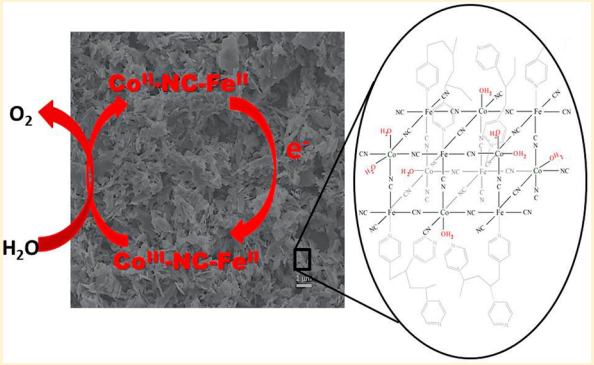

INTRODUCTION

Global energy demand is expected to double by 2050, and this level of increase cannot be met using conventional fossil-based fuels such as coal, oil, and natural gas.[1] This implicates a huge expansion in nuclear energy, which again is nonrenewable and hazardous and generates radioactive waste. There is, therefore, an urgent need to develop alternative methods for energy production that are clean and renewable.[2] Hydrogen is one of the promising candidates of renewable energy sources because it has high energy content per mass[3] and produces only water as a product.[4] One of the main bottlenecks in hydrogen economy is the development of efficient and robust water oxidation catalysts (WOCs).[5−8]

Even though metal oxides have been the primary focus,[9−16] significant efforts have also been devoted to exploring non-oxide coordination compounds in the field.[17−22] Of these, recent advances in the application of CoN_6 matrixes as WOCs created opportunity to a wide array of compounds of interest in this field.[23−28] The investigation of Prussian Blue analogues (PBAs) as WOCs by Galán-Mascarós et al. is one of the benchmark studies showing that non-oxide coordination networks could, in fact, be an alternative to cobalt oxide matrixes given their stability and robustness even in the acidic media.[29−31] The investigations of similar coordination polymers by the same group in a follow-up study[30] and a cyanide matrix with Co and Pt ions by Yamada et al. for visible-light-driven water oxidation catalysis clearly show that more studies should be performed to engage cyanide chemistry with water oxidation catalysis.[32] While metal cyanide networks in are the lead with regard to their superior stabilities, easy preparation methods, and competitive catalytic performances compared to cobalt oxides, they lag behind because of their low current densities, which could be attributed to their low number of active Co sites, also called the surface concentration. Because PBAs have surface concentration in the nmol·cm^{-2} range, a current density of 1 mA·cm^{-2} could only be achieved at higher overpotentials, above 600 mV for conventional PBAs.

The main reason for the relatively low number of active sites in cyanide systems is that most of the Co sites in the crystalline framework are connected to six N atoms of the cyanide group except the ones on the surface and the atoms inside the vacancies created to provide charge balance. It is, therefore, evident that metal cyanide networks with low or no crystallinity should be prepared to obtain a current density of 1 mA·cm^{-2} at much lower overpotentials. Because the conventional synthetic method to obtain PBAs, which involves the reaction of hexacyanometal complexes with transition-metal ions, leads to the formation of highly crystalline compounds, cyanide precursors other than hexacyanometal complexes should be

Received: January 6, 2016
Published: April 13, 2016

DOI: 10.1021/acs.inorgchem.6b00032
Inorg. Chem. 2016, 55, 4301−4307

used as precursors to reduce the crystallinity of metal cyanide networks. An important class of cyanide complexes, pentacyanoiron complexes with N-donor ligands, have widely been studied particularly in the 1980s because of their interesting optical and electrochemical properties.[33,34] They have well-established chemistry, straightforward synthetic procedures, and rich chemistry because a pentacyanoiron complex with a N-donor ligand could easily be prepared by reacting the complex $[Fe(CN)_5NH_3]^{3-}$ with a N-donor ligand such as pyridine derivatives, amino acids, amines, and even polymers with available N atoms.

Herein, it is aimed to obtain metal cyanide coordination compounds with amorphous behavior using pentacyanoferrate/poly(4-vinylpyridine) hybrid metallopolymers as precursors. The synthesis and characterization of amorphous cobalt pentacyanoferrate/poly(4-vinylpyridine) hybrid compounds are reported. Electrochemical and electrocatalytic water oxidation studies performed on the aforementioned samples deposited on a F-doped tin oxide (FTO) electrode are also the focus of this study.

EXPERIMENTAL SECTION

Synthesis. *Starting Materials.* All of the reagents and solvents were of analytical grade and were received from Sigma-Aldrich and used as such without any further processing. All solutions were prepared with deionized water (resistivity: 18 mΩ·cm).

$Na_3[Fe^{II}(CN)_5NH_3]\cdot 3H_2O$. The compound will be abbreviated as [Fe-NH_3] throughout the manuscript. It was prepared from $Na_2[Fe^{III}(CN)_5NO]\cdot 2H_2O$ (sodium nitroferricyanide) according to the procedure reported in the literature.[35] A total of 5 g of $Na_2[Fe(CN)_5NO]\cdot 2H_2O$ was dissolved in 20 mL of water. A total of 1 g of NaOH was added to the solution under constant stirring at 10 °C. A 25% (v/v) NH_4OH solution was added until saturation, followed by the addition of cold methanol.[36] The resulting yellow precipitate was aged overnight at 0 °C. The product was recrystallized using a NH_4OH/CH_3OH solution. The yield was 50%. Elem anal. Calcd for [Fe-NH_3]: C, 18.42; N, 25.78; H, 2.783. Found: C, 18.96; N, 25.34; H, 3.001. An atomic ratio of 1:3 for Fe/Na was confirmed by energy-dispersive X-ray spectroscopy (EDX). IR (cm^{-1}): 2033(s), 1619 (w), 1260 (Figure S1).

Pentacyanoferrate-Coordinated Poly(4-vinylpyridine), $Na_{15}(Fe(CN)_5)_5(C_7H_7N)_6(H_2O)_{15}$. The compound will be abbreviated as [$Fe(CN)_5$-PVP] throughout the manuscript. A synthesis similar to that in the literature was followed.[37,38] Poly(4-vinylpyridine) (200 mg), abbreviated as P4VP throughout the manuscript, was dissolved in 50 mL of methanol at room temperature. A total of 600 mg of [Fe-NH_3] was added slowly in the solution under constant stirring. After 15 min, the color of the suspension changed from yellow to orange. The reaction was allowed to continue in a covered flask for 3 days. The green precipitate was washed with methanol, followed by centrifugation (6000 rpm), to remove the unlinked pentacyanoammino complex. A total of 250 mL of cold Et_2O was added to the green $Fe(CN)_5$-*co*-P4VP suspension (approximately 50 mL) under constant stirring. The brown precipitate was isolated and dried under vacuum overnight at room temperature, resulting in a yellowish-green powder. The yield was 60%. Elem anal. Calcd for [$Fe(CN)_5$-PVP]: C, 36.99; N, 19.96; H, 3.336. Found: C, 36.43; N, 18.83; H, 3.387. An atomic ratio of 1:3 for Fe/Na was confirmed by EDX. IR (cm^{-1}): 2041, 1600, and 1417 (Figure S1). The shift observed in UV−vis spectral studies revealed the replacement of the NH_3 ligand with P4VP (Figure S2).

Cobalt Hexacyanoferrate, $K_{0.7}Co_{1.65}[Fe(CN)_6]\cdot xH_2O$. The compound will be abbreviated as [$CoFe(CN)_6$] throughout the manuscript. By using the reported drop-by-drop procedure,[39] 50 mL of a 10 mM $[Fe(CN)_6]^{4-}$ solution was prepared at room temperature. A total of 50 mL of a 20 mM $Co(NO_3)_2$ solution was added dropwise under constant stirring. The resulting bright-green solution was left under stirring for 1 h at room temperature. A total of 100 mL of acetone was added, and the suspension was centrifuged at 6000 rpm for 15 min. The precipitate was washed with an acetone/water mixture (1:1, v/v). The purification process was repeated three times. The product was collected with the addition of pure acetone and dried in an oven at 35 °C for 1 day. The yield was 73%. IR (cm^{-1}): 2080. An atomic ratio of 1:1.65 for Fe/Co was confirmed by EDX, indicating that the resulting coordination compound is $[CoFe(CN)_6]$ (Figure S3a).

Cobalt Pentacyanoferrate/Poly(4-vinylpyridine), $Co_3[Fe(CN)_5]_2$-co-P4VP·xH_2O. The compound will be abbreviated as [$CoFe(CN)_5$-PVP] throughout the manuscript. For the drop-by-drop procedure,[5] 50 mL of a 10 mM $[Fe(CN)_5]^{3-}$-*co*-P4VP solution was prepared at room temperature. A total of 50 mL of a 15 mM $Co(NO_3)_2$ solution was added dropwise under constant stirring. The resulting dark-green solution was left under stirring for 1 h at room temperature. A total of 100 mL of acetone was added, and the suspension was centrifuged at 6000 rpm for 15 min. The precipitate was washed with an acetone/water mixture (1:1, v/v). The purification process was repeated three times. The product was collected with the addition of pure acetone and dried in an oven at 35 °C for 1 day. The yield was ∼55%. IR (cm^{-1}): 2051 (Figure S1). An atomic ratio of 1:1.38 for Fe/Co was confirmed by EDX with traces of Na, indicating that the resulting coordination compound is $Co_{1.5}[Fe(CN)_5PVP]\cdot xH_2O$ (Figure S3b).

Cyanoferrate-Modified FTO Electrodes. Cobalt hexacyanoferrate modified and cobalt pentacyanoferrate/poly(4-vinylpyridine) modified FTO electrodes will be abbreviated as [$CoFe(CN)_6$@FTO] and [$CoFe(CN)_5$-PVP@FTO], respectively. A two-step in situ method was used to prepare the electrodes, which includes spin-coating the pentacyanoferrate precursor onto the FTO surface followed by dipping it in a cobalt solution. This method resulted in more stable and robust coatings of the catalyst compared to conventional methods such as drop-casting. Solutions of 0.15 M $Co(NO_3)_2\cdot 6H_2O$ and 0.1 M [$Fe(CN)_5$-PVP] were prepared with Millipore water. A [$Fe(CN)_5$-PVP] solution was spin-coated onto FTO electrodes at 1500 rpm for 2 min, resulting in a greenish-yellow translucent layer. Then, the electrode was immersed in a solution of Co^{II} for 15 min. This process was repeated twice, and the electrodes were kept in a vacuum desiccator until further use. The electrodes were rinsed with deionized water prior to use. Similar coatings were made onto FTO electrodes (at 1500 rpm for 2 min) using 0.2 M $Co(NO_3)_2\cdot 6H_2O$ and 0.1 M $[Fe(CN)_6]^{4-}$ solutions.

Physical Measurements. Elemental analyses were performed with a Thermo Scientific FLASH 2000 CHNS/O analyzer. IR spectra were measured using a Bruker ALPHA Platinum-ATR spectrometer in the wavenumber range 4000−400 cm^{-1}. UV−vis analysis was performed employing an Agilent Technologies Cary 300 UV−vis spectrophotometer. X-ray diffraction (XRD) patterns were recorded by a Panalytical X'PertPro multipurpose X-ray diffractometer employing Cu Kα radiation (λ = 1.5418 Å). Scanning electron microscopy (SEM) imaging and EDX analysis were carried out using a FEI-Quanta 200 FEG scanning electron microscope operated at 30 kV. X-ray photoelectron spectroscopy (XPS) studies were performed using a Thermo Scientific K-Alpha X-ray photoelectron spectrometer system operating with an Al Kα microfocused monochromator source ($h\nu$, 1486.6 eV; spot size, 400 mm; pass energy, 30 eV) along with a flood gun for charge neutralization. *Origin Pro 8.5* was used to plot and analyze all of the graphs.

Electrochemical Measurements. Electrochemical experiments were performed at room temperature using a Gamry Instruments Interface 1000 potentiostat/galvanostat. A conventional three-electrode electrochemical cell was used, with Ag/AgCl (3.5 M KCl) as the reference electrode, Pt wire as the counter electrode, and FTO as the working electrode (1 × 2 cm; 2 mm slides with 7 Ω·sq^{-1} surface resistivity and ∼80% transmittance). Before preparation of the electrode, the FTO slides were cleaned prior to use. Briefly, the FTO slides were washed by sonication for 15 min in a basic soapy solution, deionized water, and isopropanol, followed by annealing at 400 °C for 30 min. Buffer solutions were prepared using K_2HPO_4 and KH_2PO_4 (KPi) and adjusted by adding H_3PO_4 or KOH to the desired pH. Cyclic voltammograms were recorded in 50 mM KPi (pH 7) containing 1 M KNO_3 as electrolytes between −0.4 and +1.5 V (vs Ag/AgCl). All

DOI: 10.1021/acs.inorgchem.6b00032
Inorg. Chem. 2016, 55, 4301−4307

experiments were carried out under a N_2 atmosphere. All three electrodes were dipped in the buffer solution, and the solution was bubbled with N_2 gas for 15 min to remove the dissolved O_2 gas. The system was closed and remained closed throughout the measurement.

Bulk Water Electrolysis and Tafel Analysis. Bulk water electrolysis was performed with a two-compartment cell with a glass frit separation. Counter and reference electrodes were placed in their respective compartments. The electrolysis experiments were carried out in a KPi buffer (pH 7) solution containing 1 M KNO_3 as the supporting electrolyte. Tafel data were collected in the same conditions at different applied potentials using a steady current density of an equilibrium time of 600 s. Oxygen evolution was determined with a YSI 5100 dissolved oxygen sensing instrument equipped with a dissolved oxygen field probe inserted into the anodic compartment. A buffer solution of 130 mL was used for the electrolysis experiments. The O_2 content is recorded at STP conditions, in units of mg·L^{-1} and later converted to μmoles of O_2. EDX analysis was then performed on the electrodes to determine the atomic ratio of metal (Fe/Co) after bulk water electrolysis (Figure S4).

RESULTS AND DISCUSSION

Synthesis and Characterization. The metallopolymer, pentacyanoferrate/poly(4-vinylpyridine) [$Fe(CN)_5$-PVP], was prepared by adopting a similar synthetic approach reported previously[37] that includes the mixing of P4VP with an excess amount of $[Fe(CN)_5NH_3]^{3-}$ in methanol. IR studies performed on the compound reveal strong bands at 2041, 1600, and 1417 cm^{-1}, corresponding to the vibrational modes ν(CN), $\nu(CN_{ring})$, and $\nu(CC_{ring})$, respectively (Figure S1). The $\nu(CN_{ring})$ band at 1595 cm^{-1} of pure P4VP shifted to 1600 cm^{-1} for $[Fe(CN)_5]^{3-}$-*co*-P4VP.[38,40,41] The same trend was also noted for the $\nu(CC_{ring})$ band at 1413 cm^{-1}, which shifted to 1417 cm^{-1}.[38,40−42] The slight shift of the cyanide stretch to higher frequencies compared to the precursor (2031 cm^{-1} for [Fe-NH_3]) indicates successful substitution of the amino ligands with the P4VP group without effecting the oxidation state of the Fe centers.[38] Similarly, the shift to lower wavelengths observed in the absorbance band in UV−vis spectra also supports the formation of a metal polymer composite (Figure S2).[37,38] Moreover, the high solubility of [$Fe(CN)_5$-PVP] in water in contrast to P4VP suggests the formation of a charged polymeric species. The metal content in the sample was confirmed by EDX with an atomic ratio of 3:1 (Na/Fe), which also confirms that there is no change in the oxidation state of Fe. A molecular formula of $Na_{15}(Fe(CN)_5)_5(C_7H_7N)_6(H_2O)_{15}$ was approximated based on the atomic ratio of the metals obtained from the EDX technique and weight percentages of C, H, and N atoms obtained from CHN elemental analysis, which reveals that approximately 80% of the pyridine groups of P4VP are connected to the pentacyanoiron complex. A Co/Fe coordination polymer, [$CoFe(CN)_5$-PVP], was obtained by reacting the metallopolymer, [$FeCN_5$-PVP], with a Co^{2+} solution. Figure 1 shows the proposed structure of the amorphous compound.

In situ preparation of the metallopolymer on the FTO electrode via a two-step spin-coating method was used to improve the binding of the sample to the substrate. IR studies together with XPS and EDX studies confirm that the samples prepared on the FTO electrode by an in situ preparation method and the bulk samples are identical (Figure S5). A shift in the cyanide stretch to higher frequencies was observed, which can be attributed to the binding of a terminal N atom of the cyanide group to a Co ion. EDX of the resulting complex showed an Fe/Co ratio in good agreement with that of the bulk complex.

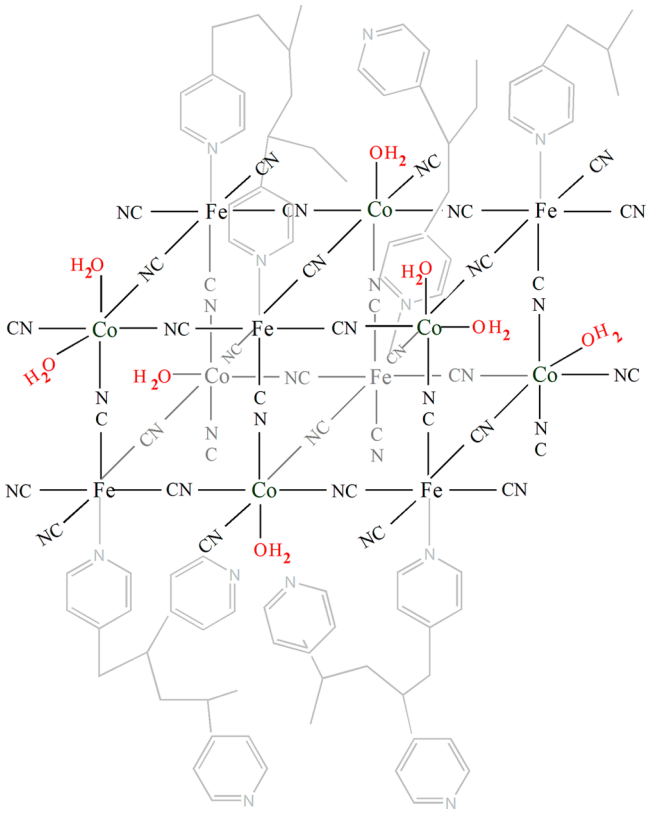

Figure 1. Proposed structure for the cobalt pentacyanoferrate/poly(4-vinylpyridine) catalyst [$CoFeCN_5$-PVP].

Electrochemistry. Electrochemical and electrocatalytic studies were performed at pH 7 using a standard phosphate buffer in the presence of 1 M KNO_3. Cyclic voltammetry of [$CoFe(CN)_5$-PVP] deposited on the FTO electrode (denoted as [$CoFe(CN)_5$-PVP@FTO]) was recorded in the −0.4 to −1.8 V range with respect to a Ag/AgCl reference electrode (Figure 2). It exhibits two main features: (i) a quasi-reversible redox couple with an oxidation peak at 0.46 V and a reduction peak at 0.26 V versus the Ag/AgCl reference electrode ($E_{1/2}$ = 0.36 V; $E_c - E_a$ = 200 mV), which is attributed to the Co^{2+}/Co^{3+} redox couple; (ii) an irreversible peak that corresponds to the catalytic water oxidation process. A similar study was also performed with the [$CoFe(CN)_6$@FTO] electrode (Figure S6). A slight increase in the peak-to-peak separation of the Co^{2+}/Co^{3+} redox couple was observed with increasing scan rate due to uncompensated solution resistance (3.8 Ω), which was obtained from the slope of the linear relationship between the peak-to-peak separation and peak current (Figure S7). From the slope of the linear peak current versus the scan rate plot, the surface concentration of Co sites in [$CoFe(CN)_5$-PVP@FTO] was calculated as 13.8 nmol·cm^{-2}, while it is 2 nmol·cm^{-2} for the [$CoFe(CN)_6$@FTO] electrode (Figures S8 and S9). The dramatic increase in the number of active Co sites with respect to cobalt hexacyanoferrate can be attributed to the limiting effect of the polymeric moiety on the dimensionality of the network. The polymeric group serves not only as a capping ligand by binding to each Fe center but also as a surfactant because of its chain structure. The size of the cyanide network is confined to ∼5 Å, which is the length of a Fe−CN−Co binding mode, in at least one dimension because all of the pentacyanoiron groups are connected to the polymeric chain,

DOI: 10.1021/acs.inorgchem.6b00032
Inorg. Chem. 2016, 55, 4301−4307

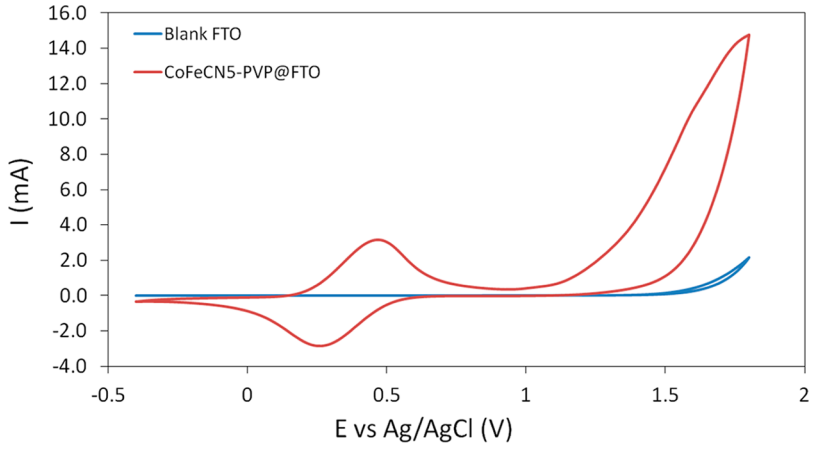

Figure 2. Cyclic voltammogram of the [$CoFe(CN)_5$-PVP@FTO] electrode recorded in a 50 mM KPi electrolyte at pH 7.0 (red line) with a 25 mV·s^{-1} sweep rate. Electrochemical response of a blank FTO electrode (blue line).

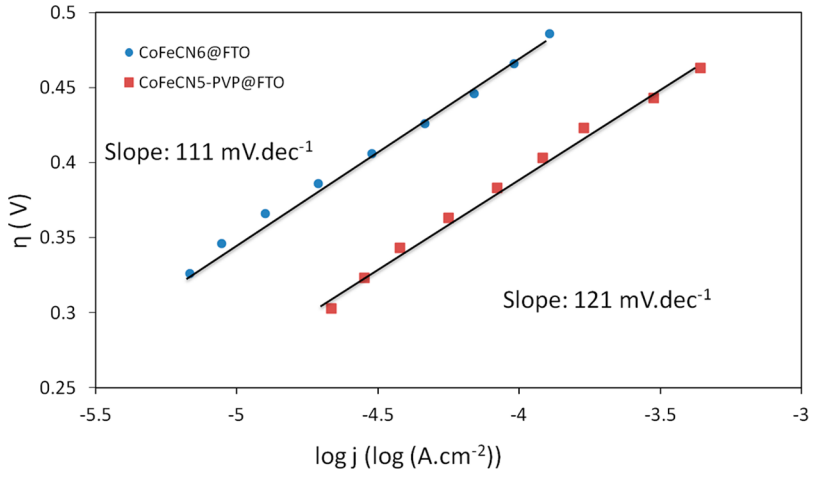

Figure 3. Tafel plots for the [$CoFe(CN)_6$@FTO] (blue circles) and [$CoFe(CN)_5$-PVP@FTO] (red squares) electrodes from 0.9 to 1.1 V versus Ag/AgCl electrode recorded in a 50 mM KPi electrolyte at pH 7.0.

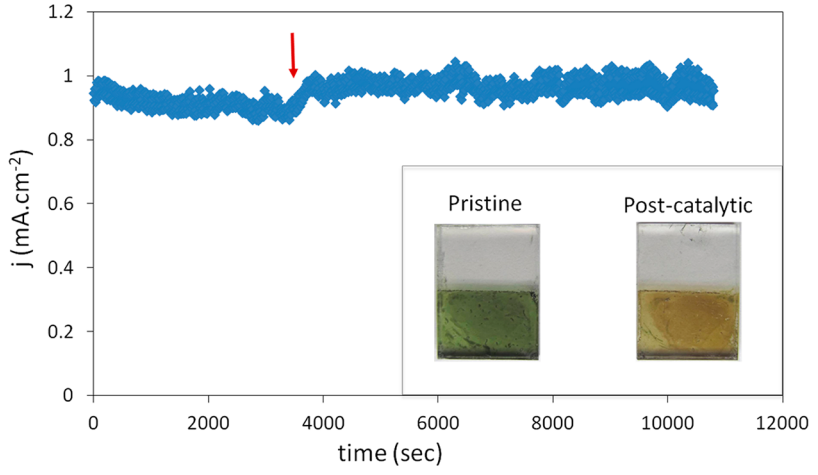

Figure 4. Chronoamperometry measurement of the [$CoFe(CN)_5$-PVP@FTO] electrode at 1.2 V versus Ag/AgCl in a KPi buffer at pH 7. The red arrow indicates the mechanical removal of bubbles. The inset shows the images of the electrodes before and after the catalytic process.

leading to approximately a 7-fold increase in the number of active Co sites.

For evaluation of the catalytic activities of modified electrodes, chronoamperometric measurements were performed to measure the current densities at different overpotentials (Figure 3). The current densities obtained by the [$CoFe(CN)_6$@FTO] electrode are in good accordance with those in the previous study.[29] A Tafel slope (111 mV·dec^{-1}) higher than that reported by Galán-Mascarós et al. (88 mV·dec^{-1}) was observed because of the use of different deposition

DOI: 10.1021/acs.inorgchem.6b00032
Inorg. Chem. 2016, 55, 4301−4307

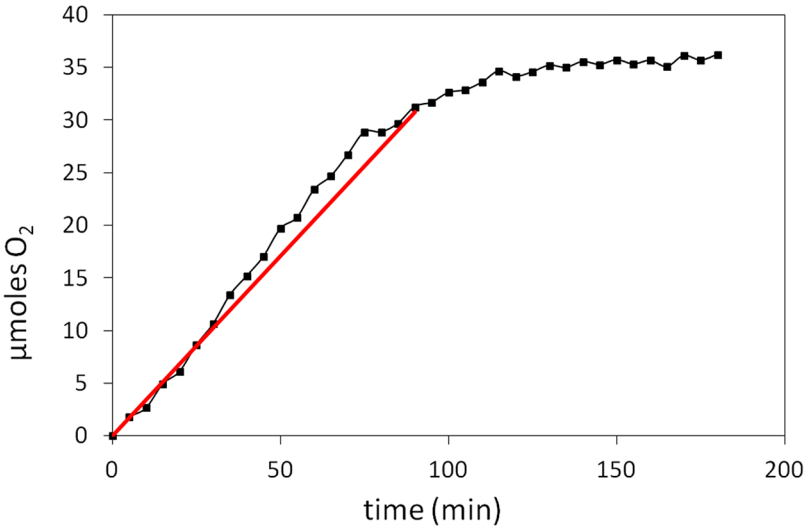

Figure 5. Faradaic efficiency of [$Fe(CN)_5$-PVP@FTO] measured by an oxygen-sensor system. Bulk electrolysis was performed at 1.2 V versus Ag/AgCl in a gastight electrochemical cell. The amount of dissolved O_2 molecules detected during bulk electrolysis and the theoretical amount of evolved O_2 assuming a Faradaic efficiency of 100% are represented by the black and red lines, respectively.

techniques resulting in a higher amount of catalyst loading. A linear relationship between log j and the overpotential was obtained in an overpotential range of 300−500 mV with respect to the Ag/AgCl reference electrode. A deviation from linearity at higher overpotentials is observed as a result of the formation of oxygen bubbles, which limits mass transport on the electrode surface (Figure S10). Furthermore, a catalytic onset potential of 360 mV is required to produce a current density of 55 $\mu A \cdot cm^{-2}$, which is in the range of those obtained for other Co-based catalysts (for Co/Pi, η = 280 mV; η = 310 mV for $Co(PO_3)_2$, η = 434 mV for Co_3O_4, and η = 310 mV for CoNCN).[43−45] Although [$CoFe(CN)_5$-PVP@FTO] exhibits a higher Tafel slope than [$CoFe(CN)_6$@FTO], a significant improvement in the current densities was observed. A current density of 1 $mA \cdot cm^{-2}$ could be achieved at η = 510 mV for [$CoFe(CN)_5$-PVP@FTO], while the same current density could be obtained above η > 600 mV for [$CoFe(CN)_6$@FTO], mainly as a result of the difference in the number of active Co sites. To check the long-term stability of the catalyst, bulk electrolysis was performed with both [$CoFe(CN)_5$-PVP@FTO] (Figure S11) and [$CoFe(CN)_6$@FTO] (Figure S12) over 2 days at 1.2 V versus Ag/AgCl, with regular intervals leaving the electrodes in the electrolyte solution. Similar behavior was observed for both of the samples, where a gradual decrease in the current density initially is observed, followed by a consistent stable current density at each step. The initial decrease could be attributed to the leaching of poorly attached particles from the FTO electrode.

A turnover frequency (TOF) of 2.6 × 10^{-3} s^{-1} could be achieved at overpotentials of 262 and 284 mV, respectively, for [$CoFe(CN)_6$@FTO] and [$CoFe(CN)_5$-PVP@FTO] (Figure S13). The similarity in the log TOF versus η plots indicates that active Co sites have similar coordination spheres, as expected. The quantity of O_2 produced during bulk electrolysis of modified FTO electrodes at a constant potential of 1.2 V was also monitored for 3 h. A stable current density of ∼1 $mA \cdot cm^{-2}$ was obtained, which suggests the stability of the electrodes during electrolysis over 3 h (Figure 4). The quantity of dissolved O_2 measured by an oxygen-sensing instrument reached saturation after 2 h. A similar behavior was also observed with the [$CoFe(CN)_6$@FTO] electrode with a relatively lower current density (450 $\mu A \cdot cm^{-2}$; Figure S14), which resulted in a longer time (around two and half hours) to reach saturation compared to that of [$CoFe(CN)_5$-PVP@FTO] (Figure S15). A theoretical fit that yields the quantity of oxygen calculated using Faraday's law for a $4e^-$ process matches the experimental slope for oxygen evolution, suggesting that the origin of the increase in the current is water oxidation (Figure 5).

Characterization of Electrodes. Characterization studies were also performed for electrodes after bulk electrolysis at 1.2 V versus Ag/AgCl. SEM imaging was performed on the [$CoFe(CN)_5$-PVP@FTO] electrodes to investigate the morphology of the coating (Figure 6). The image suggests that the

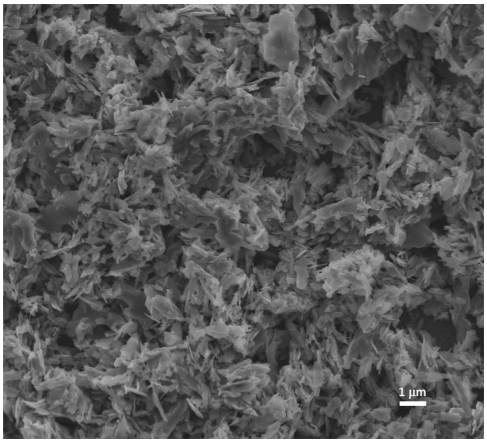

Figure 6. SEM image of the [$CoFe(CN)_5$-PVP@FTO] electrode.

coating is consistent with no long-term orderliness, which also explains the amorphous nature of the catalyst (XRD pattern in Figures S16 and S17). The coating exhibits submicron-sized catalyst particles distributed uniformly all over the electrode surface.

A color change from green to brown as a result of partial oxidation of Co sites was observed during electrolysis. IR and XPS studies were performed to investigate the behavior of

DOI: 10.1021/acs.inorgchem.6b00032
Inorg. Chem. 2016, 55, 4301−4307

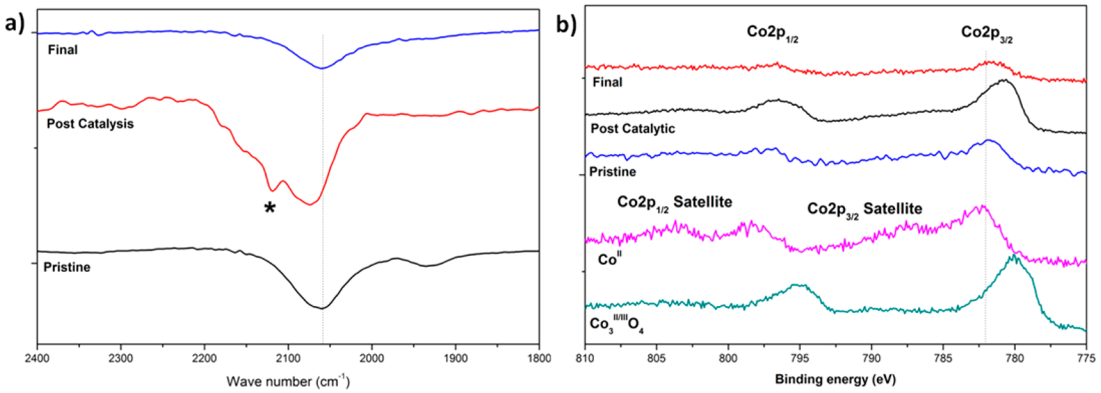

Figure 7. (a) IR spectra of the [$CoFe(CN)_5$-PVP@FTO] electrode before (pristine), after 3 h of bulk electrolysis (postcatalytic), and after a reduction potential of −200 mV is applied for 30 min to the postcatalytic electrode (final) in a KPi buffer solution at pH 7. The peak represented with an asterisk is attributed to the oxidized Fe^{II}−CN−Co^{III} binding mode. (b) XPS spectra of the Co 2p region of the surface of the pristine, postcatalytic, and final electrodes. The spectra for Co_3O_4 and $Co(NO_3)_2$ were also depicted as references.

partial oxidation as well as the stabilities of the electrodes. IR studies performed on the catalyst scraped from the electrode after electrolysis revealed an additional stretch corresponding to Fe^{II}−CN−Co^{III} at 2116 cm^{-1} as a result of partial oxidation of Co sites (Figure 7a). The presence of the intense asymmetric band at 2059 cm^{-1} in both the original and postcatalytic samples suggests that the oxidation of Co sites is partial. XPS analysis was performed to further study the oxidation state of the Co sites in the original and postcatalytic electrodes (Figure 7b). The Co $2p_{3/2}$ line at 781.88 eV of the original electrode is observed to be in close accordance with that of Co^{II} salt (782.28 eV). Additionally, a strong satellite band associated with the Co $2p_{3/2}$ line at 4−8 eV above the principle band was observed. Likewise, the Co $2p_{1/2}$ line positioned at 796.68 eV in the pristine sample, slightly chemically shifted from the line corresponding to Co $2p_{1/2}$ in the Co^{II} salt (798.38 eV), is readily identifiable. An additional satellite associated with the Co $2p_{1/2}$ line at 5−6 eV above the principle line was observed. Each of the principle lines exhibits strong bands with scalable full width at half-maxima (fwhm; >3.5 eV) suitable for identification. Satellite lines associated with Co $2p_{3/2}$ and Co $2p_{3/2}$ were, however, broad and, hence, not suitable for identification purposes. In the postcatalytic sample, the Co $2p_{3/2}$ and Co $2p_{1/2}$ lines were observed at 780.58 and 796.48 eV, respectively, which are slightly lower than the binding energies observed for the original sample. Both of the lines exhibit strong bands with a scalable fwhm (>4 eV) and, hence, suitable for identification. The Co 2p lines for Co^{II} and Co^{III} generally fall very close or may even overlap and, thus, are generally difficult to differentiate. Earlier studies, however, focused on differentiating Co^{II} from Co^{III} by observing the satellite bands of the Co 2p lines; high-spin Co^{II} ions have intense or scalable satellite bands, whereas low-spin Co^{III} ions have very weak or missing satellite bands. In the postcatalytic sample, very weak to almost negligible satellite bands were observed, indicating that the sample most likely is low-spin Co^{III}. Therefore, it can be safely concluded that the top layer of the electrode exhibits some degree of oxidation in the postcatalytic sample considering the XPS and IR results.

XPS and IR studies were also performed on the postcatalytic electrodes that were treated with a reduction potential of −200 mV to test the reversibility of the catalytic cycle. It was observed that the color of the samples turned back to green, which is the color of the original sample. Moreover, a shoulder in the IR spectrum and peaks that correspond to Co^{III} ions in XPS disappeared after treatment with the reduction potential. Both IR and XPS spectra are identical with those of the original electrodes. It is, therefore, evident that the catalyst retains its structure during the catalytic process and that oxidation of Co sites is a reversible process. XPS of the O 1s line (Figure S18) was also observed to investigate the stability of the electrodes. Spectra of both the original and postcatalytic samples exhibit peaks that are attributed to the surface-adsorbed oxygen species. No persistent O 1s bands are found at binding energies lower than 530 eV that correspond to lattice oxygen species in either of the samples, confirming the absence of any oxide-based species before and after catalysis. Decomposition of cyanide-based clusters to form any Co-based oxides was, thus, ruled out based on comparative XPS studies performed on electrodes and the reference Co_3O_4 compound.

CONCLUSIONS

Several non-oxide coordination networks including Co/Fe PBAs have recently been investigated for their electrocatalytic and photocatalytic water oxidation performances. Extended networks with $\{CoN_6\}$ moieties have progressed in the field thanks to the higher TOFs obtained by Co sites surrounded with N atoms compared to cobalt oxide systems and their robustness and stabilities in both acidic and neutral media. Non-oxide cobalt systems, however, exhibit low current densities as a result of their low surface concentrations. The synthetic method reported herein aimed to improve the number of active Co sites while retaining the chemical nature of individual Co sites (Co atoms surrounded with terminal N atoms of bridging cyanide groups) in Co−Fe Prussian Blue coordination compounds.

Metallopolymers with pentacyanoiron complexes can be ideal candidates as precursors for amorphous coordination compounds with promising electrocatalytic activities. A metallopolymer with dangling cyanide groups serves as a suitable medium not only to obtain $\{CoN_6\}$ moieties but also to avoid long-range ordering of metal cyanometalate clusters because of the presence of polymeric chains, which results in an improvement in the number of active Co sites.

Comparable TOFs of [$CoFe(CN)_6$@FTO] and [$CoFe(CN)_5$-PVP@FTO] electrodes (a TOF value of 2.6×10^{-3} s^{-1} could be achieved at overpotentials of 262 and 284 mV, respectively, for [$CoFe(CN)_6$@FTO] and [$CoFe(CN)_5$-PVP@

DOI: 10.1021/acs.inorgchem.6b00032
Inorg. Chem. 2016, 55, 4301−4307

FTO]) are mainly a result of the same type of network structural motif including the Fe−CN−Co type of binding groups, thus similar coordination spheres for active Co sites. A current density of 1 $mA{\cdot}cm^{-2}$ was obtained at much lower overpotentials (η = 510 mV) with a $CoFe(CN)_5$-PVP-modified FTO electrode as expected mainly as a result of approximately a 7-fold increase in the number of active Co sites with respect to a conventional cobalt hexacyanoferrate system.

Two disciplines of chemistry, pentacyanometal complexes and water oxidation, have been engaged for the first time. Because pentacyanometal complexes have well-established chemistry, straightforward synthetic procedures, and rich chemistry due to the diversity of N-donor ligands, the strategy outlined in this project will also be used to introduce a series of robust and efficient catalysts to the field of water oxidation. Furthermore, the effect of the surface area on the availability of active metal sites and the activity of the catalyst needs more emphasis.

■ ASSOCIATED CONTENT

Supporting Information

The Supporting Information is available free of charge on the ACS Publications website at DOI: 10.1021/acs.inorgchem.6b00032.

IR spectra, UV−vis spectra in solution, EDX spectra, cyclic voltammograms, Tafel plots, TOF plots, XRD patterns, and XPS spectra (PDF)

■ AUTHOR INFORMATION

Corresponding Author

*E-mail: karadas@fen.bilkent.edu.tr.

Notes

The authors declare no competing financial interest.

■ ACKNOWLEDGMENTS

The authors thank the Science and Technology Council of Turkey, TUBITAK (Project 114Z473), for financial support.

■ REFERENCES

(1) Hoffert, M. I.; Caldeira, K.; Jain, A. K.; Haites, E. F.; Harvey, L. D.; Potter, S. D.; Schlesinger, M. E.; Schneider, S. H.; Watts, T. M. L.; Wigley, T. M. L.; Wuebbles, D. J. *Nature* **1998**, *395*, 881−884.

(2) Lewis, N. S.; Nocera, D. G. *Proc. Natl. Acad. Sci. U. S. A.* **2006**, *103*, 15729−15735.

(3) Jena, P. *J. Phys. Chem. Lett.* **2011**, *2*, 206−211.

(4) Durbin, D. J.; Malardier-Jugroot, C. *Int. J. Hydrogen Energy* **2013**, *38*, 14595−14617.

(5) Barber, J. *Chem. Soc. Rev.* **2009**, *38*, 185−196.

(6) Sartorel, A.; Carraro, M.; Toma, F. M.; Prato, M.; Bonchio, M. *Energy Environ. Sci.* **2012**, *5*, 5592−5603.

(7) Shin, S.-M.; Jung, J.-Y.; Park, M.-J.; Song, J.-W.; Lee, J.-H. *J. Power Sources* **2015**, *279*, 151−156.

(8) Blankenship, R. E.; Tiede, D. M.; Barber, J.; Brudvig, G. W.; Fleming, G.; Ghirardi, M.; Gunner, M. R.; Junge, W.; Kramer, D. M.; Melis, A.; Moore, T. A.; Moser, C. C.; Nocera, D. G.; Nozik, A. J.; Ort, D. R.; Parson, W. W.; Prince, R. C.; Sayre, R. T. *Science* **2011**, *332*, 805−809.

(9) Harriman, A.; Pickering, I. J.; Thomas, J. M.; Christensen, P. A. *J. Chem. Soc., Faraday Trans. 1* **1988**, *84*, 2795−2806.

(10) Risch, M.; Grimaud, A.; May, K. J.; Stoerzinger, K. A.; Chen, T. J.; Mansour, A. N.; Shao-Horn, Y. *J. Phys. Chem. C* **2013**, *117*, 8628−8635.

(11) Frey, C. E.; Wiechen, M.; Kurz, P. *Dalton Trans.* **2014**, *43*, 4370−4379.

(12) Li, W.; Sheehan, S. W.; He, D.; He, Y.; Yao, X.; Grimm, R. L.; Brudvig, G. W.; Wang, D. *Angew. Chem., Int. Ed.* **2015**, *54*, 11428−11432.

(13) Nocera, D. G. *Acc. Chem. Res.* **2012**, *45*, 767−776.

(14) Smith, R. D. L.; Prévot, M. S.; Fagan, R. D.; Zhang, Z.; Sedach, P. A.; Siu, M. K. J.; Trudel, S.; Berlinguette, C. P. *Science* **2013**, *340*, 60−63.

(15) Wasylenko, D. J.; Palmer, R. D.; Berlinguette, C. P. *Chem. Commun.* **2013**, *49*, 218−227.

(16) Smith, R. D. L.; Prévot, M. S.; Fagan, R. D.; Trudel, S.; Berlinguette, C. P. *J. Am. Chem. Soc.* **2013**, *135*, 11580−11586.

(17) Xue, L.-X.; Meng, T.-T.; Yang, W.; Wang, K.-Z. *J. Photochem. Photobiol., B* **2015**, *152*, 95−105.

(18) Brimblecombe, R.; Dismukes, G. C.; Swiegers, G. F.; Spiccia, L. *Dalton Trans.* **2009**, 9374−9384.

(19) Maeda, K.; Domen, K. *J. Phys. Chem. C* **2007**, *111*, 7851−7861.

(20) Bloomfield, A. J.; Sheehan, S. W.; Collom, S. L.; Anastas, P. T. *ACS Sustainable Chem. Eng.* **2015**, *3*, 1234−1240.

(21) Liu, H.; Schilling, M.; Yulikov, M.; Luber, S.; Patzke, G. R. *ACS Catal.* **2015**, *5*, 4994−4999.

(22) Wang, J.; Li, K.; Zhong, H.-x.; Xu, D.; Wang, Z.-l.; Jiang, Z.; Wu, Z.-j.; Zhang, X.-b. *Angew. Chem.* **2015**, *127*, 10676−10680.

(23) Zhao, W.; Liu, Y.; Liu, J.; Chen, P.; Chen, I. W.; Huang, F.; Lin, J. *J. Mater. Chem. A* **2013**, *1*, 7942−7948.

(24) Masa, J.; Xia, W.; Sinev, I.; Zhao, A.; Sun, Z.; Grützke, S.; Weide, P.; Muhler, M.; Schuhmann, W. *Angew. Chem., Int. Ed.* **2014**, *53*, 8508−8512.

(25) Wang, Y.; Ding, W.; Chen, S.; Nie, Y.; Xiong, K.; Wei, Z. *Chem. Commun.* **2014**, *50*, 15529−15532.

(26) Pfrommer, J.; Lublow, M.; Azarpira, A.; Göbel, C.; Lücke, M.; Steigert, A.; Pogrzeba, M.; Menezes, P. W.; Fischer, A.; Schedel-Niedrig, T.; Driess, M. *Angew. Chem., Int. Ed.* **2014**, *53*, 5183−5187.

(27) Ressnig, D.; Shalom, M.; Patscheider, J.; More, R.; Evangelisti, F.; Antonietti, M.; Patzke, G. R. *J. Mater. Chem. A* **2015**, *3*, 5072−5082.

(28) Chen, Y.; Fu, L.; Liu, Z. *Chem. Commun.* **2015**, *51*, 16637−16640.

(29) Pintado, S.; Goberna-Ferrón, S.; Escudero-Adán, E. C.; Galán-Mascarós, J. R. *J. Am. Chem. Soc.* **2013**, *135*, 13270−13273.

(30) Goberna-Ferrón, S.; Hernández, W. Y.; Rodríguez-García, B.; Galán-Mascarós, J. R. *ACS Catal.* **2014**, *4*, 1637−1641.

(31) Galán-Mascarós, J. R. *ChemElectroChem* **2015**, *2*, 37−50.

(32) Yamada, Y.; Oyama, K.; Gates, R.; Fukuzumi, S. *Angew. Chem., Int. Ed.* **2015**, *54*, 5530−5530.

(33) Macartney, D. H. *Rev. Inorg. Chem.* **1988**, *9*, 101−151.

(34) Lee, G.-H.; Della Ciana, L.; Haim, A. *J. Am. Chem. Soc.* **1989**, *111*, 2535−2541.

(35) Brauer, G. *Handbook of Preparative Inorganic Chemistry*, 2nd ed.; Academic Press Inc.: New York, 1963; Vol. *1*.

(36) Kenney, D. J.; Flynn, T. P.; Gallini, J. B. *J. Inorg. Nucl. Chem.* **1961**, *20*, 75−81.

(37) Liu, Y.; Wang, X. *Polym. Chem.* **2012**, *3*, 2632−2639.

(38) Jannuzzi, S. A. V.; Martins, B.; Felisberti, M. I.; Formiga, A. L. B. *J. Phys. Chem. B* **2012**, *116*, 14933−14942.

(39) Roy, X.; Hui, J. K. H.; Rabnawaz, M.; Liu, G.; MacLachlan, M. J. *J. Am. Chem. Soc.* **2011**, *133*, 8420−8423.

(40) Zhou, X.; Goh, S. H.; Lee, S. Y.; Tan, K. L. *Polymer* **1997**, *38*, 5333−5338.

(41) Valkama, S.; Hartikainen, J.; Torkkeli, M.; Serimaa, R.; Ruokolainen, J.; Rissanen, K.; ten Brinke, G.; Ikkala, O. *Macromol. Symp.* **2002**, *186*, 87−92.

(42) Sheng, K.; Yan, B. *J. Mater. Sci.: Mater. Electron.* **2010**, *21*, 65−71.

(43) Ahn, H. S.; Tilley, T. D. *Adv. Funct. Mater.* **2013**, *23*, 227−233.

(44) Biesinger, M. C.; Payne, B. P.; Grosvenor, A. P.; Lau, L. W. M.; Gerson, A. R.; Smart, R. S. C. *Appl. Surf. Sci.* **2011**, *257*, 2717−2730.

(45) Surendranath, Y.; Kanan, M. W.; Nocera, D. G. *J. Am. Chem. Soc.* **2010**, *132*, 16501−16509.

DOI: 10.1021/acs.inorgchem.6b00032
Inorg. Chem. 2016, 55, 4301−4307